

Article

Initiation of Infrasonic Geosphere Waves Caused by Explosive Eruption of Hunga Tonga-Hunga Ha‘apai Volcano

Grigory Dolgikh *, Stanislav Dolgikh * and Vladimir Ovcharenko

V.I. Il'ichev Pacific Oceanological Institute, Far Eastern Branch Russian Academy of Sciences,
690041 Vladivostok, Russia; ovcharenko@poi.dvo.ru

* Correspondence: dolgikh@poi.dvo.ru (G.D.); sdolgikh@poi.dvo.ru (S.D.)

Abstract: The paper presents the results of processing recordings of abnormal signals, which originated during the eruption of Hunga Tonga-Hunga Ha‘apai volcano, and were registered by a laser nanobarograph and two laser strainmeters; there were three meters of sea-level variations, located in the Sea of Japan, and twelve meters of sea-level variations, located in the Pacific Ocean. Acoustic-gravity Lamb waves, generated in the atmosphere, caused disturbances of similar periods in the Earth's crust, which were registered by laser strainmeters. Atmospheric impulse and Lamb waves during their propagation over the Pacific Ocean and the Sea of Japan initiated meteorological tsunamis in their waters, at periods corresponding to the seiches (Eigen oscillations) of registration stations' location areas. In the records of all sea wave recorders, we did not find signs of a classical tsunami origination, and in the records of laser strainmeters, we did not find signals corresponding to seabed displacements at the point of the volcano explosion that led to the formation of a classical tsunami.

Keywords: volcano; explosion; laser nanobarograph; laser strainmeters; Lamb wave; meteorological tsunami; tsunami



Citation: Dolgikh, G.; Dolgikh, S.; Ovcharenko, V. Initiation of Infrasonic Geosphere Waves Caused by Explosive Eruption of Hunga Tonga-Hunga Ha‘apai Volcano. *J. Mar. Sci. Eng.* **2022**, *10*, 1061. <https://doi.org/10.3390/jmse10081061>

Academic Editor: Efim Pelinovsky

Received: 24 June 2022

Accepted: 29 July 2022

Published: 2 August 2022

Publisher's Note: MDPI stays neutral with regard to jurisdictional claims in published maps and institutional affiliations.



Copyright: © 2022 by the authors. Licensee MDPI, Basel, Switzerland. This article is an open access article distributed under the terms and conditions of the Creative Commons Attribution (CC BY) license (<https://creativecommons.org/licenses/by/4.0/>).

1. Introduction

When studying geosphere processes of a wide frequency range, it is important to solve problems of identifying the primary source of registered oscillations and waves, and specifying patterns of their transformation at the boundary of geospheres. Therefore, for an adequate interpretation of the obtained results, research on one of the geospheres must be accompanied by research on neighboring geospheres, including study of the fields of a different nature [1,2]. In the linear case, this interaction can be observed for processes of identical frequencies, and in the nonlinear case—during the interaction of geosphere fields of different frequency ranges [3]. Nonlinear cases are of particular interest from the point of view of an abrupt change in the state of the medium at a threshold energy accumulation and trigger effect on the medium [4]. Energy transition is possible not only within fields of the same nature, but also between fields of a completely different nature, not related to each other at first glance. To study the peculiarities of inter-geosphere interaction and the patterns of energy transfer from one process to another, we need long-term complex interdisciplinary observations of natural geosphere processes, followed by their processing, analysis, and interpretation. In linear cases, this is extremely difficult to do. Nonlinear processes are interesting because of their enormous energy and, therefore, we can study inter-geosphere interactions and the patterns of these processes' transformation at the boundary of geospheres in a much shorter time than in linear cases. Nonlinear cases can be created artificially, for example, by explosions, operation of various powerful seismoacoustic and hydroacoustic emitters, MHD-generators (MHD), etc. Natural initiation of nonlinear processes can be associated with the occurrence of catastrophic phenomena and processes. Such natural catastrophic processes include earthquakes, tsunamis, tornadoes and cyclones, volcano eruptions, etc.

From the point of view of the initiation of various geosphere processes with inter-geosphere energy transfer, an interesting event occurred on 15 January 2022, on Hunga Tonga-Hunga Ha‘apai Island in the Tonga archipelago, which appeared as a result of volcanic activity in 2014–2015 [5]. On 20 December 2021, an eruption of the volcano began on the island, and on 15 January at 04:15 UTC, the eruption went into the active explosive phase, at the final stage of which, the volcano exploded [6]. The central part of the volcano’s caldera with an area of approximately 5 km² was located at depths from 150 to 200 m. This explosion led to the release into the stratosphere of a huge amount of water vapor, according to the analysis of measurements of the Microwave Limb Sounder (MLS) [7]. The power of the explosion was 10 megatons in TNT equivalent. Analysis of records from the sensors, located in the Pacific Ocean along the path of the atmospheric impulse of the explosion (see Figure 1), shows that the propagation velocities of these disturbances for all receiving points were approximately equal to the speed of sound in the air. It testifies to the fact that the signal from the eruption site to the registration points came through the air, and not through the water. That is, the recorded signals relate rather to meteorological tsunamis, caused by atmospheric disturbances, and created by a powerful explosion. These disturbances were recorded by nanobarographs at a distance of several thousand kilometers from the volcano [8]. Along with the impulse in the atmosphere, while analyzing satellite data, we found atmospheric gravity waves, formed as a result of the vertical movement of particles from the sea surface into the ionosphere [9,10].

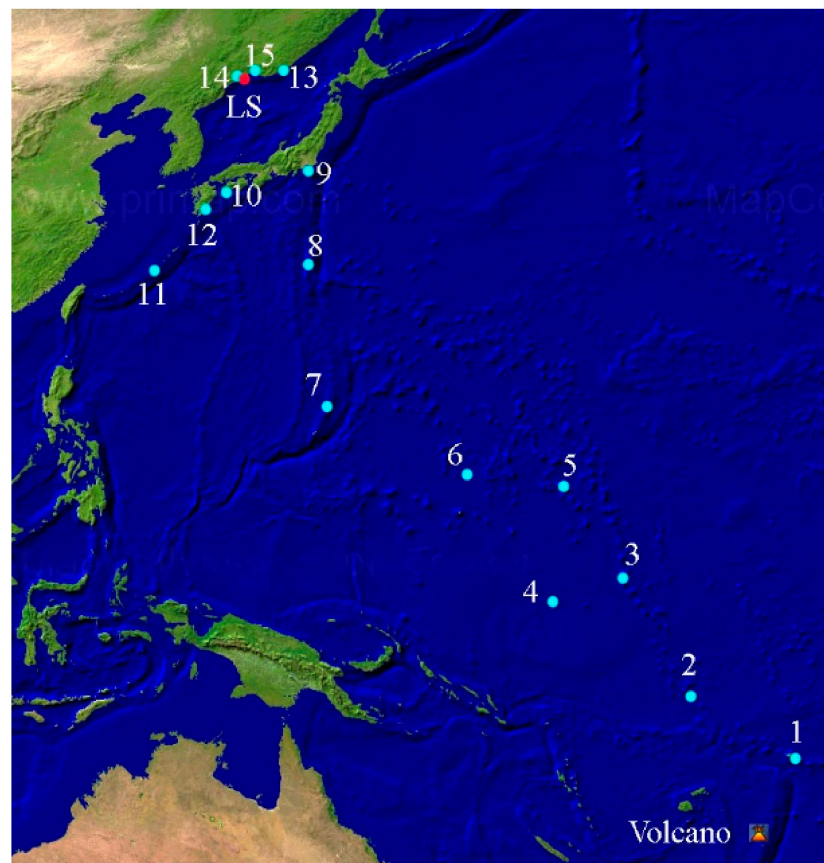


Figure 1. 1–12 show stations in the Pacific Ocean; 13–15—stations in the Sea of Japan near the coast of the Primorsky Territory of Russia. Red circles mark the location of the laser-interference receiving systems.

The atmospheric impulse of the volcano explosion spread throughout the planet. However, after passing over the registration points (shown in Figure 1) in the Pacific Ocean, it spread to the Sea of Japan, where the effects of its impact on the atmosphere, the water

surface, and the Earth's crust were recorded. At three points in the Sea of Japan, marked in Figure 1, the receiving stations recorded water surface oscillations, caused by the impact of this impulse. At Schultz Cape in the Sea of Japan, the explosion impulse, and the further oscillations caused by it, were recorded by a laser nanobarograph [11], which records atmosphere pressure variations, and by two laser strainmeters [12], designed to record deformation variations in the upper layer of the Earth's crust at their location.

In the following sections of the paper, we will briefly describe the laser nanobarograph and the laser strainmeters, and will pay great attention to the processing and interpretation of the experimental data, obtained from the laser nanobarograph, the laser strainmeters, and all receiving systems, marked in Figure 1.

2. Laser-Interference Receiving Systems

Figure 2 shows the appearance of the laser nanobarograph, created on the base of an equal-arm Michelson interferometer, a frequency-stabilized helium-neon laser by Melles Griott, which ensures frequency stability in the ninth digit, a block of aneroid boxes with mirror coating, a digital registration system, and a block for transmitting the obtained data to the experimental database. All the laser nanobarographs we created register atmosphere pressure variations in the frequency range from 0 (conditionally) to 10,000 Hz, with an accuracy of 50 μPa .

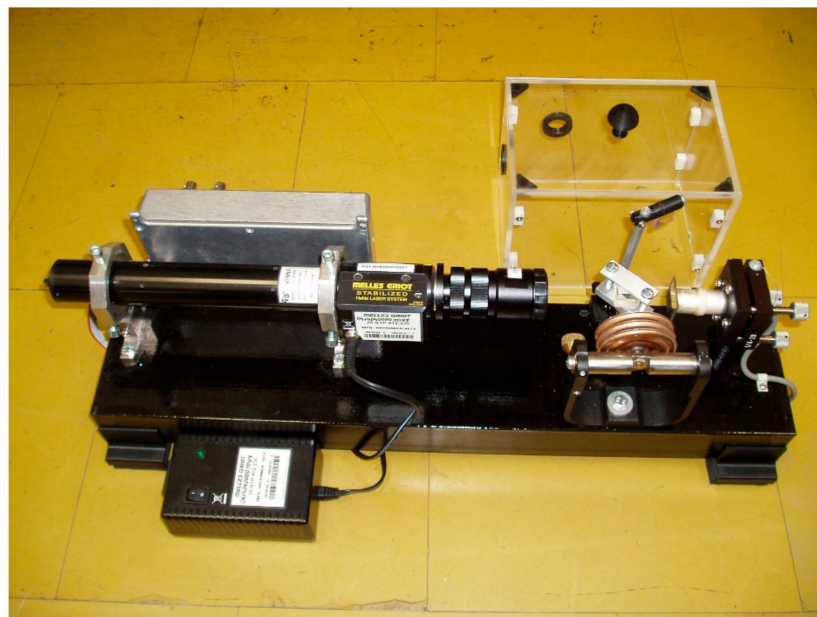


Figure 2. Laser nanobarograph.

The two-coordinate laser strainmeter consists of two unequal-arm laser strainmeters: a 52.5-meter “north–south” laser strainmeter and a 17.5-meter “west–east” laser strainmeter. The “north–south” laser strainmeter, the working arm of which is oriented at the angle of 18° to the “north–south” line, created on the basis of an unequal-arm Michelson interferometer and a frequency-stabilized helium-neon laser, is located at the depth of 3–5 m below the Earth's surface. The “west–east” laser strainmeter is mounted at a distance of 70 m from this laser strainmeter, at the depth of 3–4 m from the Earth's surface. Its working arm is oriented at the angle of 110° to the “north–south” line. The angle between the working axes of the laser strainmeters is 92° . Using interferometry methods, we can record changes in the length of the working arm of each strainmeter with an accuracy of 0.01 nm, i.e., the measuring accuracy of the displacement variations in the strainmeters' abutments is 0.01 nm. Figure 3 schematically shows the measuring site at Schultz Cape. The laser nanobarograph is also located underground, in one of the cabinets of the 52.5-meter laser strainmeter.



Figure 3. Number 1 is the 52.5-meter laser strainmeter, 2—17.5-meter laser strainmeter. 3—laboratory building.

In real-time mode, all information, obtained from these devices, after preliminary processing (filtration and decimation), is transferred to the laboratory room, where, with a sampling frequency of up to 2 kHz, it is recorded on hard media of the experimental database.

3. Processing and Analysis of the Obtained Experimental Data

We started by processing the obtained experimental data with data from the laser nanobarograph, the device that recorded the atmospheric pressure variations, caused by the atmospheric impulse, generated during the volcano explosion. We started with the laser nanobarograph data because they are the only data that accurately describe atmosphere pressure variations caused by the explosion, and also the waves it generated. As we will show further, it is the atmosphere processes that play the main role in generating oscillations and waves that occurred in the Earth's crust and in the water environment, and was associated with the volcano explosion. The laser nanobarograph and the laser strainmeters registered several passages of atmospheric disturbances caused by the volcano explosion. We can see both Lamb waves and the impulse, generated during the explosion of the volcano, in the records of all instruments.

Figure 4 presents the laser nanobarograph record, which shows the impulse, generated during the volcano explosion, and the acoustic-gravity Lamb waves, initiated by it. This record corresponds to the first passage of the disturbance signal. We processed a fragment of the laser nanobarograph record with a duration of 4096 s (sampling frequency 1 Hz), starting immediately after the noted impulse. As a result of processing by the periodogram method, we formed a spectrum, a part of which is shown in Figure 5. In the figure, we can identify four powerful peaks with periods of 17 min 04.0 s (amplitude—13.2 Pa), 8 min 32.0 s (amplitude—8.2 Pa), 4 min 16.0 s (amplitude—7.7 Pa), 3 min 06.2 s (amplitude—5.3 Pa), and a peak with a period of 1 min 42.4 s (amplitude—2.8 Pa).

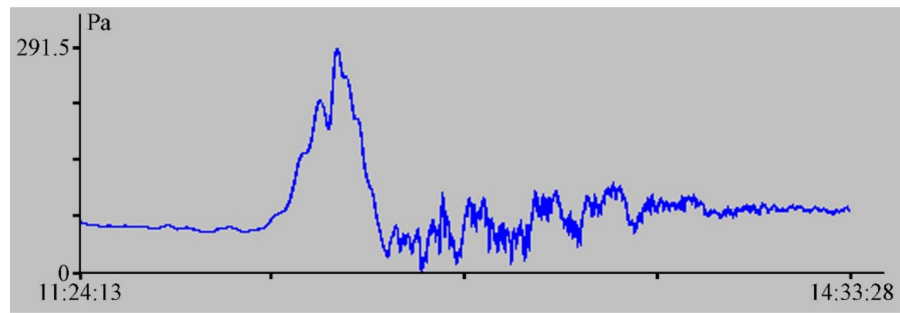


Figure 4. Fragment of laser nanobarograph record for 15 January 2022, UTC.

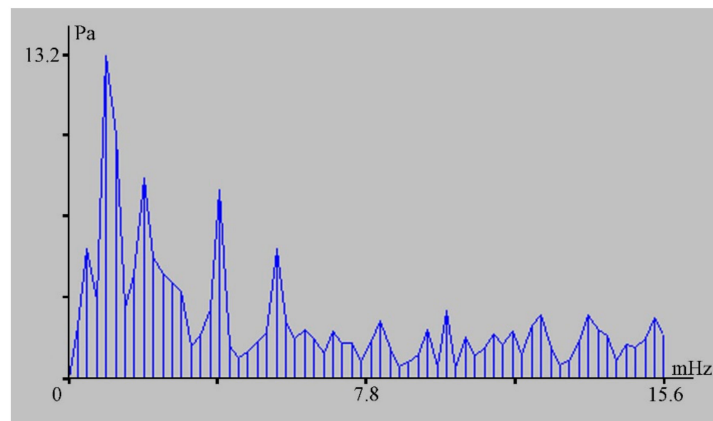


Figure 5. Spectrum of laser nanobarograph record fragment with duration of 4096 s.

The atmospheric pressure impulse and acoustic-gravity Lamb waves caused deformations of a similar type in the Earth’s crust (see Figures 6 and 7). In the figures, an impulse in the Earth’s crust caused by the acoustic-gravity Lamb wave is highlighted in red, and 4096 seconds after the pulse is highlighted in green; these were further analyzed.

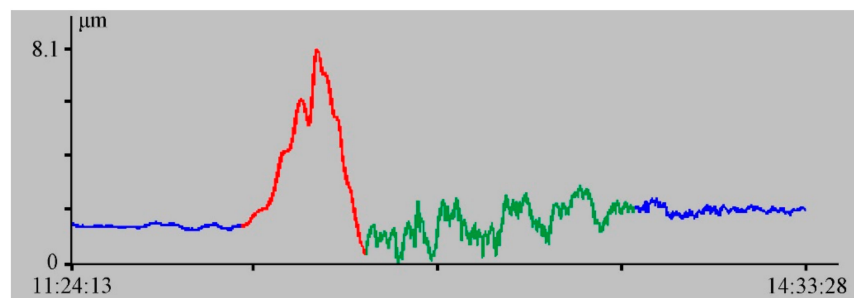


Figure 6. Fragment of “north–south” laser strainmeter record for 15 January 2022, UTC.

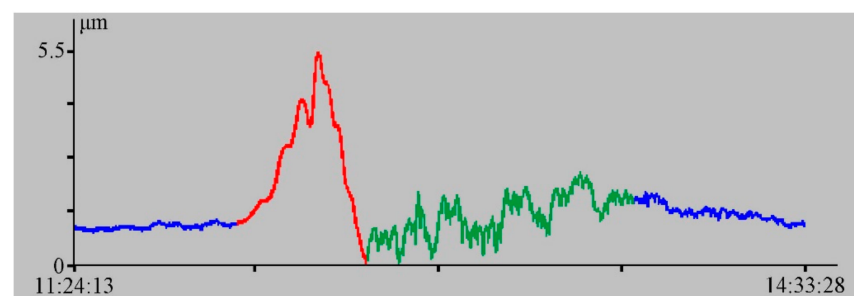


Figure 7. Fragment of “west–east” laser strainmeter record for 15 January 2022, UTC.

Table 1 lists the spectral maxima, obtained from processing synchronous records of the laser nanobarograph, the “north–south” laser strainmeter, and the “west–east” laser strainmeter. The duration of each fragment is 4096 s; the sampling frequency is 1 Hz.

Table 1. Data of spectral processing of records of the laser-interference systems, installed at Schulz Cape, the first direct passage of Lamb waves near Schultz Cape.

	17 min 04 s	8 min 32 s	4 min 16 s	3 min 6.2 s
Nanobarograph	13.2 Pa	8.2 Pa	7.7 Pa	5.3 Pa
“North–south” laser strainmeter	0.39 μm	0.23 μm	0.20 μm	0.13 μm
“West–east” laser strainmeter	0.26 μm	0.17 μm	0.15 μm	0.095 μm

During the first antipodal passage, we identified the spectral maxima, listed in Table 2. The duration of the processed fragment is 4096 s; the sampling frequency is 1 Hz. All fragments were processed using the fast Fourier transform that does not allow good frequency resolution to be obtained. Wherein, the harmonics corresponding to periods of 17 min 04.0 s and 13 min 39.2 s are near, and, depending on the recording quality, the presence of other powerful energy-significant processes in the records, a peak with a period of 17 min 04.0 s or a peak with a period of 13 min 39.2 s, may stand out; although, they probably refer to the same process.

Table 2. Data of spectral processing of records of the laser-interference systems, installed at Schulz Cape, the antipodal passage of Lamb waves near Schultz Cape.

	13 min 39.2 s	8 min 32 s
Nanobarograph	5.8 Pa	2.5 Pa
“North–south” laser strainmeter	0.18 μm	0.087 μm
“West–east” laser strainmeter	0.12 μm	0.053 μm

When processing the data of the laser nanobarograph and the laser strainmeters after the second direct passage of this disturbance, we identified the spectral maxima, listed in Table 3. The duration of the processed fragment is 4096 s; the sampling frequency—1 Hz.

Table 3. Data of spectral processing of records of the laser-interference systems, installed at Schulz Cape, the second direct passage of Lamb waves near Schultz Cape.

	17 min 4 s	8 min 32 s
Nanobarograph	6.2 Pa	2.5 Pa
“North–south” laser strainmeter	0.19 μm	0.073 μm
“West–east” laser strainmeter	0.11 μm	0.057 μm

Let us assume that initiated are modes with periods of 17 min 04.0 s, 8 min 32.0 s, and 4 min 16.0 s, corresponding to the Lamb wave modes in the region of observation. The conclusion that the oscillations with a period of, for example, 17 min 04.0 s belong to the region of observation can be drawn from analysis of other laser nanobarograph records, obtained at other times, and not related to the volcano explosion. Figure 8 shows a record of the above laser nanobarograph, obtained at this test site in 2016. Spectral processing of this record also showed a powerful peak with a period of about 17 min 04.0 s, see Figure 9.

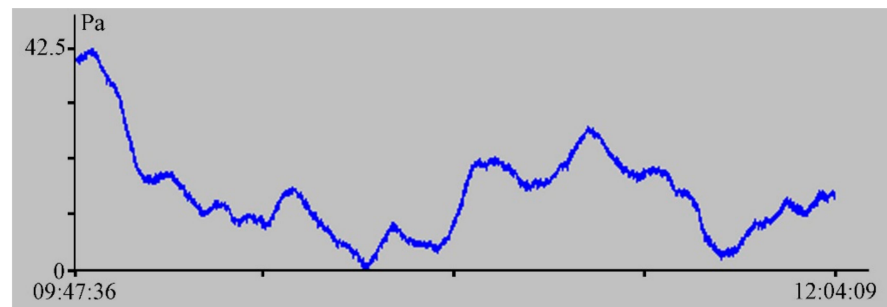


Figure 8. Fragment of laser nanobarograph record for 1 March 2016, UTC.

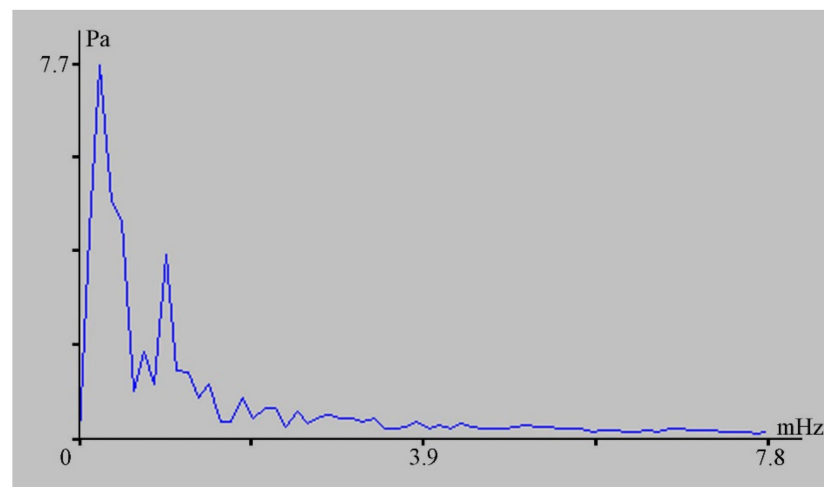


Figure 9. Spectrum of the laser nanobarograph record fragment, shown in Figure 8.

Let us now briefly discuss the spectral maximum with a period of 3 min 06.2 s, which does not fit into the series of spectral maxima, related to the Lamb wave modes. This spectral maximum was previously identified in the records of the laser strainmeters, located at Schultz Cape [13]. Powerful spectral components at periods of about 3 min stand out while processing the records of the laser strainmeters, installed in an underground mine near the city of Krasnokamensk and on Taiwan Island [13–15]. Previously, we assumed that oscillations with a period of about 3 min in the records of three spaced-apart laser strainmeters are associated with bending oscillations of the Earth's crust [15]. As we can see from the material described above, these spectral maxima are present in the laser nanobarograph records. It testifies to the fact that the primary source of these oscillations is in the atmosphere, and, possibly, is due to edge waves, associated with the surface layers of the atmosphere. Of course, we cannot deny the possibility of atmosphere oscillation initiation by the Earth's oscillatory processes, by analogy with the initiation of atmosphere oscillations by Eigen oscillations of the Earth at the corresponding periods [16]. Perhaps, the transformation coefficient of the laser nanobarograph data to the laser strainmeter data will shed light on the nature of these oscillations. For the periods listed in Table 1, it equals: 17 min 04.0 s ($13.2 \text{ Pa}/0.39 \mu\text{m} = 33.8 \text{ Pa}/\mu\text{m}$), 8 min 32.0 s ($8.2 \text{ Pa}/0.23 \mu\text{m} = 35.0 \text{ Pa}/\mu\text{m}$), 4 min 16.0 s ($7.7 \text{ Pa}/0.2 \mu\text{m} = 38.5 \text{ Pa}/\mu\text{m}$), and 3 min 06.2 s ($5.3/0.13 \mu\text{m} = 40.8$). Such behavior of the transformation coefficient (increase with period decreasing) indicates that the source of all the identified oscillations is in the atmosphere.

Now, let us analyze the records of instruments that record sea-level variations on the way from the volcano to the laser-interference systems, located at Schultz Cape in the Sea of Japan, at the point with coordinates 42.5810°N , 131.1564°E . Figure 1 shows a map with information on stations, located in the Pacific Ocean and in the Sea of Japan; the sea can be considered closed from tsunami waves from the Pacific Ocean. Figure 10 shows fragments of records of sea receiving systems, marked by numbers 1–15 in Figure 1. Most

of these sensors of OBP records of sea levels are made by AANDERAA and Valeport with a level measurement accuracy of $\pm 0.2\%$ of the measurement range. The data are taken from sites [17,18].

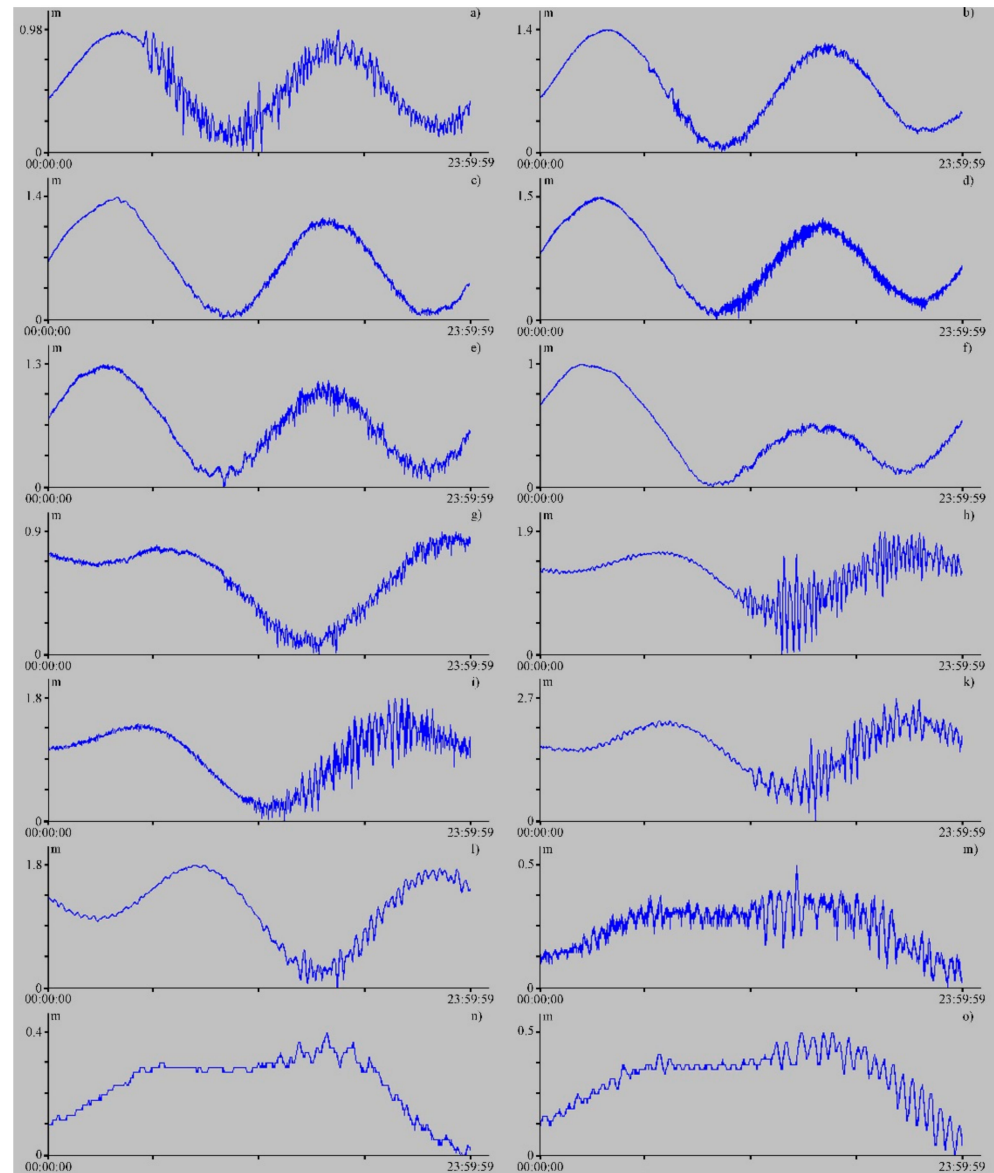


Figure 10. Record fragments of sea-level meters at stations: (a) Apia Upolu WS, (b) Fongafale p, (c) Betio Tarawa, (d) Nauru, (e) Kwajalein, (f) Dekehtik Pohnpei, (g) Saipan, (h) Chichijima, (i) Mera, (k) Tosashimizu, (l) Naha, (m) Preobrazhenije, (n) Pos'et, (o) Vladivostok. For 15 January 2022, UTC.

The beginning of the disturbances, shown on all stations' graphs, coincides with the arrival of an atmospheric impulse, caused by the volcano explosion, with a speed approximately equal to the speed of sound in the air. In refs. [19,20], it is stated that, along with sea-level variations, caused by this atmospheric impulse and formed by Lamb waves, the stations, located in the Pacific Ocean, recorded tsunami waves, resulting from the volcano explosion. These tsunami waves should originate as a result of water masses movement, caused by the movement of particular areas of the marine Earth's crust at the volcano explosion point. The oscillations of the Earth's crust, which are recorded by stand-alone seismographs, described in ref. [20], being the same as oscillations that occur in the hypocenter during any tsunamigenic earthquake, do not cause a tsunami. Tsunamis originate from significant displacements of the upper layer of the marine Earth's

crust, which are not recorded even by the widest-band seismographs. They are recorded by devices that have unique amplitude–frequency characteristics and allow recording displacements starting from 0 (conditionally) Hz, that is—laser strainmeters [21]. As shown in ref. [21], these systems register displacements of the sea/ocean bottom, leading to tsunami origination, at almost any planetary distance.

Next, we will focus on the analysis of the record fragments, shown in Figure 10, and on looking in the records of one of the laser strainmeters, described in the previous section, for a deformational disturbance, which led to the origination of the tsunami, described in refs. [19,20]. Let us start with an analysis of the data, shown in Figure 10.

Table 4 lists the results of spectral processing of experimental data from the stations in the first column. The following designations are introduced in the table: the first column shows the sea signal recording stations; the second column shows the names of the fragments in the background period and during the recording of disturbance signals; columns 3 to 5 show the periods of the identified maxima, the values of relative amplitudes, and calculated propagation velocity of the disturbance signal from the volcano to the registration point. Coinciding maxima are highlighted in color. The duration of each processed data fragment was 4096 s at a sampling frequency of 1 Hz. The processing method was the fast Fourier transform. During processing, two fragments were selected for each station—the background (before the arrival of a disturbance signal), and the fragment with a disturbance signal. What is the most important? The data of fourteen stations were processed, out of which the spectral maxima were identified at nine stations, with periods coinciding with the maxima of the background observation periods. It testifies to the fact that the initiation of these signals occurred during the arrival of the air impulse resulting from the volcano explosion.

Table 4. Statistics of the results of background data and disturbance signal data processing.

Station		Maximum1	Maximum2	Maximum3	Velocity, m/s
Apia Upolu WS	Background	1 h 04 min 13 s (0.002)	25 min 41.4 s (0.0016)	18 min 21.0 s (0.0015)	
	Signal	11 min 56.9 s (0.032)	30 min 13.4 s (0.027)	18 min 21.0 s (0.021)	218
Fongafale	Background	42 min 48.9 s (0.0014)	8 min 01.7 s (0.0011)	6 min 35.2 s (0.00098)	
	Signal	9 min 52.8 s (0.0092)	42 min 48.9 s (0.0086)	20 min 33.1 s (0.0053)	209
Betio Tarawa	Background	32 min 02.7 s (0.0056)			
	Signal	32 min 02.7 s (0.0068)	7 min 25.8 s (0.0051)	10 min 03.2 s (0.0046)	212
Nauru	Background	51 min 22.7 s (0.0015)	39 min 31.3 s (0.0013)	13 min 53.2 s (0.001)	
	Signal	6 min 15.9 s (0.0045)	36 min 41.9 s (0.0043)	28 min 32.6 s (0.0039)	222
Kwajalein	Background	58 min 48.5 s (0.0026)	5 min 14.4 s (0.0024)	37 min 48.3 s (0.0022)	
	Signal	13 min 55.7 s (0.014)	48 min 07.0 s (0.011)	9 min 37.4 s (0.0089)	235
Dekehtik Pohnpei	Background	56 min 58.1 s (0.0017)	16 min 01.3 s (0.00077)	5 min 53.6 s (0.00051)	
Saipan	Background	56 min 51 s (0.0019)	23 min 15.4 s (0.0017)	7 min 12.4 s (0.0013)	
	Signal	11 min 53.9 s (0.011)	9 min 50.4 s (0.011)	13 min 49.7 s (0.01)	279
Chichijima	Background	20 min 28.0 s (0.0055)	16 min 30.3 s (0.0051)	13 min 49.7 s (0.003)	
	Signal	20 min 28.0 s (0.12)	15 min 02.9 s (0.091)	12 min 47.5 s (0.043)	286
Mera	Background	6 min 09.9 s (0.0051)	5 min 19.8 s (0.0047)	22 min 14.7 s (0.0044)	
	Signal	22 min 14.7 s (0.11)	6 min 05.5 s (0.044)	6 min 38.7 s (0.042)	290
Tosashimizu	Background	20 min 28.0 s (0.015)	39 min 21.4 s (0.0072)		

Table 4. *Cont.*

Station		Maximum1	Maximum2	Maximum3	Velocity, m/s
Naha	Signal	20 min 28.0 s (0.14)	24 min 21.8 s (0.11)	42 min 38.2 s (0.054)	290
	Background	26 min 55.7 s (0.008)			
	Signal	24 min 21.8 s (0.057)	10 min 26.5 s (0.011)		
Preobrazhenije	Signal	22 min 14.7 s (0.11)	25 min 34.9 s (0.089)	19 min 40.7 s (0.067)	288
	Background D	31 min 58.7 s (0.01)	15 min 59.3 s (0.0035)		
Pos'et	Signal	30 min 05.8 s (0.033)	9 min 28.5 s (0.011)	15 min 59.3 s (0.0074)	293
	Background	31 min 58.7 s (0.0029)	17 min 38.6 s (0.0018)	10 min 53.2 s (0.0012)	
	Signal	30 min 05.8 s (0.0072)	17 min 38.6 s (0.0035)	11 min 22.2 s (0.0012)	287
Vladivostok	Background	39 min 21.4 s (0.0081)	31 min 58.7 s (0.0062)		
	Signal	31 min 58.7 s (0.032)			286

If we believe that, along with the atmospheric disturbance that led to a meteorological tsunami origination, the volcano explosion should result in a classical tsunami, we can look for this disturbance in the records of stations, shown in Figure 10. It is difficult to understand how fast a classical tsunami wave should propagate. Let us calculate this speed in accordance with the expression $v = \sqrt{gh}$ at depths of 2000 or 4000 m. The delay of a classical tsunami, compared to a meteorological tsunami, for each receiving station, listed in Table 4, will be:

- **Apia Upolu WS**—from 37 min 54 s to 6 min 52 s.
- **Fongafale**—from 1 h 05 min to 6 min 46 s.
- **Betio Tarawa**—from 1 h 53 min 51 s to 15 min 39 s.
- **Nauru**—from 2 h 12 min 07 s to 27 min 21 s.
- **Kwajalein**—from 3 h 03 min 21 s to 50 min 30 s.
- **Dekehtik Pohnpei**—from 3 h 41 min 16 s to 1 h 12 min 26 s.
- **Saipan**—from 5 h 48 min 31 s to 2 h 23 min 36 s.
- **Chichijima**—from 7 h 08 min 51 s to 3 h 02 min 46 s.
- **Mera**—from 8 h 02 min 25 s to 3 h 29 min 13 s.
- **Tosashimizu**—from 8 h 21 min 09 s to 3 h 37 min 20 s.
- **Naha**—from 8 h 15 min 38 s to 3 h 33 min 07 s.

Upon careful examination of the fourteen cited stations’ records, we could not find signals, corresponding to a tsunami, which came along the water surface from the point of the volcano explosion.

4. Conclusions

When processing the records of the laser nanobarograph and two laser strainmeters, located at the Marine Experimental Station “Schulz Cape” on the Sea of Japan coast, we noted three direct passages and one antipodal passage of the atmospheric impulse, and Lamb waves, formed as a result of Hunga Tonga-Hunga Ha ‘apai volcano explosion. We established that oscillations of the Earth’s crust at the location of the laser strainmeters and identified in their records at periods of 17 min 04.0 s, 8 min 32.0 s, and 4 min 16.0 s are caused by Lamb waves, generated by the impulse, formed as a result of the volcano explosion. We showed that the Lamb wave with a period of 17 min 04.0 s has a regional origin and was observed at other times during the initiation of atmosphere processes. Oscillations close to the period of 3 min 06.2 s are recorded in various regions of the planet (Transbaikalia (Russia), the Primorsky Territory (Russia), Taiwan). The primary source of all selected wave processes is in the atmosphere.

During its propagation over the Pacific Ocean waters in each region, the atmospheric impulse generated its own oscillations of water masses (seiches) in the recording equipment

locations. In the Sea of Japan, in addition to local seiches, the seiches of the Sea of Japan were initiated in the period range of 30 min 05.8 s to 31 min 58.7 s; they were noted at all stations, located in the Sea of Japan. We believe that the periods of the identified maxima correspond to the known resonant frequencies of the atmosphere, which are excited by the disturbance.

Author Contributions: G.D.—problem statement, discussion, and writing of the article. S.D.—data processing, discussion, and writing the article. V.O.—data curation, visualization. All authors have read and agreed to the published version of the manuscript.

Funding: The work was financially supported by the Russian Science Foundation, project No. 22-17-00121 “Origin, development and transformation of geosphere processes in infrasonic range”.

Institutional Review Board Statement: Not applicable.

Informed Consent Statement: Informed consent was obtained from all subjects involved in the study.

Data Availability Statement: Third Party Data. Restrictions apply to the availability of these data.

Acknowledgments: We would like to express our deep gratitude to all employees of the Physics of Geo-spheres laboratory.

Conflicts of Interest: The authors declare no conflict of interest.

References

1. Adushkin, V.V.; Spivak, A.A. Near-surface geophysics: Complex investigations of the lithosphere-atmosphere interactions. *Izv. Phys. Solid Earth* **2012**, *48*, 181–198. [CrossRef]
2. Adushkin, V.V.; Spivak, A.A. Problems related to the interaction of geospheres and physical fields in near-surface geophysics. *Izv. Phys. Solid Earth* **2019**, *55*, 1–11. [CrossRef]
3. Shalimov, S.L.; Nesterov, I.A.; Vorontsov, A.M. On the GPS-based ionospheric perturbation after the Tohoku earthquake of 11 March 2011. *Izvestiya. Phys. Solid Earth*. **2017**, *53*, 262–273. [CrossRef]
4. Adushkin, V.V.; Kocharyan, G.G. Trigger processes in geosystems. *Izv. Phys. Solid Earth* **2011**, *47*, 259–261. [CrossRef]
5. Garvin, J.B.; Slayback, D.A.; Ferrini, V.; Frawley, J.; Giguere, C.; Asrar, G.R.; Andersen, K. Monitoring and Modeling the Rapid Evolution of Earth’s Newest Volcanic Island: Hunga Tonga Hunga Ha’apai (Tonga) Using High Spatial Resolution Satellite Observations. *Geophys. Res. Lett.* **2018**, *45*, 3445–3452. [CrossRef]
6. Zhao, W.; Sun, C.; Guo, Z. Reawakening of Tonga volcano. *Innovation* **2022**, *3*, 100218. [CrossRef] [PubMed]
7. Xu, J.; Li, D.; Bai, Z.; Tao, M.; Bian, J. Large Amounts of Water Vapor Were Injected into the Stratosphere by the Hunga Tonga–Hunga Ha’apai Volcano Eruption. *Atmosphere* **2022**, *13*, 912. [CrossRef]
8. Brodsky, E.; Lay, T. The wave blown around the world. *Science* **2022**, *377*, 30–31. [CrossRef] [PubMed]
9. Adam, D. Tonga Volcano Eruption Created Puzzling Ripples in Earth’s Atmosphere. *Nature* **2022**, *601*, 497. [CrossRef]
10. Vergoz, J.; Hupe, P.; Listowski, C.; Le Pichon, A.; Garcés, M.; Marchetti, E.; Labazuy, P.; Ceranna, L.; Pilger, C.; Gaebler, P.; et al. IMS observations of infrasound and acoustic-gravity waves produced by the January 2022 volcanic eruption of Hunga, Tonga: A global analysis. *Earth Planet. Sci. Lett.* **2022**, *591*, 117639. [CrossRef]
11. Dolgikh, G.I.; Dolgikh, S.G.; Kovalev, S.N.; Koren, I.A.; Novikova, O.V.; Ovcharenko, V.V.; Okuntseva, O.P.; Shvets, V.A.; Chupin, V.A.; Yakovenko, S.V. A laser nanobarograph and its application to the study of pressure-strain coupling. *Izv. Phys. Solid Earth* **2004**, *40*, 683–691.
12. Dolgikh, G.I.; Kovalev, S.N.; Koren, I.A.; Ovcharenko, V.V. A Two-Coordinate Laser Strainmeter. *Izv. Phys. Solid Earth* **1988**, *34*, 946–950.
13. Dolgikh, G.I.; Chupin, V.A.; Yu-Hung, H. Photon Antenna “Russia-Taiwan”. *Photonics* **2018**, *12*, 586–597. [CrossRef]
14. Dolgikh, G.I.; Dolgikh, S.G.; Rasskazov, I.Y.; Lugovoy, V.A.; Saksin, B.G. A 50-m laser strainmeter system installed in Transbaikalia: Testing results. *Russ. Geol. Geophys.* **2016**, *57*, 1771–1777. [CrossRef]
15. Dolgikh, G.I.; Dolgikh, S.G.; Chupin, V.A.; Yu-Hung, H. The Nature of Terrestrial Infragravitational “Noise”. *Dokl. Earth Sci.* **2016**, *471*, 1257–1260. [CrossRef]
16. Shved, G.M.; Petrova, L.N.; Polyakova, O.S. Penetration of the Earth’s free oscillations at 54 minute period into the atmosphere. *Ann. Geophys.* **2000**, *18*, 566–572. [CrossRef]
17. Available online: <http://www.ioc-sealevelmonitoring.org/map.php> (accessed on 20 January 2022).
18. Available online: <http://www.rtw.su/sea-level/> (accessed on 20 January 2022).

19. Kulichkov, S.N.; Chunchuzov, I.P.; Popov, O.E.; Gorchakov, G.I.; Mishenin, A.A.; Perepelkin, V.G.; Bush, G.A.; Skorokhod, A.I.; Vinogradov, Y.A.; Semutnikova, E.G.; et al. Acoustic-Gravity Lamb Waves from the Eruption of the Hunga-Tonga-Hunga-Hapai Volcano, Its Energy Release and Impact on Aerosol Concentrations and Tsunami. *Pure Appl. Geophys.* **2022**, *179*, 1533–1548. [[CrossRef](#)]
20. Matoza, R.S.; Fee, D.; Assink, J.D.; Iezzi, A.M.; Green, D.N.; Kim, K.; Toney, L.; Lecocq, T.; Krishnamoorthy, S.; Lalande, J.-M.; et al. Atmospheric waves and global seismoacoustic observations of the January 2022 Hunga eruption, Tonga. *Science* **2022**, *377*, 95–100. [[CrossRef](#)] [[PubMed](#)]
21. Dolgikh, G.I.; Dolgikh, S.G. Deformation Anomalies Accompanying Tsunami Origination. *J. Mar. Sci. Eng.* **2021**, *9*, 1144. [[CrossRef](#)]